Journal of Materials Chemistry A

ROYAL SOCIETY OF CHEMISTRY

PAPER

View Article Online
View Journal | View Issue

Check for updates

Cite this: J. Mater. Chem. A, 2025, 13, 8816

Pseudo-lithium vacancies in hydrogen rich Li_3OCl†

Benjamin A. D. Williamson, * Kristoffer Eggestad and Sverre M. Selbach

Received 25th November 2024
Accepted 14th February 2025

DOI: 10.1039/d4ta08352k

rsc.li/materials-a

The antiperovskite Li_3OCl is reported as a superionic conductor, however, reproducibility has been poor due to its hygroscopic nature, suggesting that reports are in fact on $Li_{3-x}OH_xCl$. Most experimental and computational studies in the literature focus on pure Li_3OCl however, and do not take into account the role of hydrogen in the material. Here, we develop a full defect model of H-doped Li_3OCl, showing that the nominal Schottky disorder diminishes with hydrogen incorporation. Additionally, H helps to facilitate Li-ion mobility in Li_3OCl by firstly introducing rotatable OH species as well as forming H_{Li} which relaxes off site to form what we define as a "pseudo-V_{Li}" enhancing the ionic conductivity in line with experimentally observed values. Intentional hydrogen doping of hygroscopic materials constitute an underexplored strategy for enhancing ionic transport properties.

Open Access Article. Published on 18 February 2025. Downloaded on 2/20/2026 10:03:46 PM. This article is licensed under a Creative Commons Attribution 3.0 Unported Licence.

1. Introduction

Electrochemical energy storage has become an increasingly vital component of modern society ever present in both portable electronics and transportation, as well as becoming important in the realisation of a full renewable energy grid. The dominating type of rechargeable battery rely on Li-ions which intercalate into an anode upon charging, typically graphitic,[1] migrate back to a cathode (for example: $LiCoO_2$,[2] $LiFePO_4$ (ref. 3 and 4) (LFP), or $LiNi_xMn_yCo_{1-x-y}O_2$ (NMC)[5]) upon discharging, and a liquid/polymer electrolyte such as LiTFSI.[6] These electrolytes typically possess desirable conductivities[7] of the order of 10^{-2} S cm^{-1}. However, they present significant safety risks due to their flammable nature. Further disadvantages are formation of potentially rate limiting solid-electrolyte interphases, simultaneous anion diffusion,[8] lower operating voltages,[9] and (dendrite formation causing incompatibility with Li-metal anodes with ~10× the capacity of current graphitic anodes[10]).[11] The use of a solid-state electrolyte (SSE) is therefore desirable as it fixes many of these problems simultaneously.

Current solid electrolyte materials include *e.g.* the Li-rich garnets such as $Li_7La_3Zr_2O_{12}$ (LLZO),[12–14] the Argyrodites Li_6MS_5X (M = S, Se, X = Cl, Br, I),[15–17] $Li_{10}GeP_2S_{12}$ (LGPS),[18–20] as well as $Li_xP_yO_zN$ (LiPON).[21,22] Unfortunately, these materials possess a tradeoff between stability and conductivity. LiPON, for example, possesses excellent electrochemical stability and resistance towards dendrite formation,[23] (yet poor/mediocre conductivities of the order of 10^{-6} S cm^{-1} are typically observed[21]), making it suitable for small scale devices or as a protective layer in conventional lithium battery cells.[24] Whilst a lower conductivity would intuitively be expected in the solid state compared to the liquid state, competitively high conductivities (>10^{-3} S cm^{-1}) are observed for some solid state materials.[25] However, some expected issues do arise with respect to stability and synthesis of these materials.[8,26]

Within the past decade, Li-rich anti-perovskites, such as Li_3OCl have gained a lot of interest due to their initial high reported ionic conductivities at ambient conditions (10^{-3} S cm^{-1}) as reported by Zhao and Daemen.[27] Subsequent experimental and density functional theory (DFT) studies, however, have placed the conductivity to be much lower with a higher migration barrier (~0.6 eV and 10^{-6} S cm^{-1} (ref. 28 and 29)). Both nominally Li_3OCl and Li_3OBr have been shown to possess wide electrochemical stability windows even if they are metastable and not in a global ground state. This has been attributed to not possessing additional cations that may be reduced by Li-metal, yet may form Li_2O and LiCl/Br at the anode.[30] Additional antiperovskite ionic conductor compositions have been reported including, Na_3OCl/Br,[31,32] Na_3SI[33] and Na_3HS[34] to name a few.

Despite promising electrochemical stability and sometimes promising ionic conductivities, Li_3OCl is a hygroscopic and air sensitive material.[29] This has raised numerous questions on the legitimacy of Li_3OCl as the true composition, with consensus trending towards the fact that Li_3OCl being a hydrated form ($Li_{3-x}OH_xCl$) or even Li_2OHCl.[29,35] In a critical review by Rettenwander and coworkers,[35] they point out the fact that typical syntheses of Li_3OCl uses LiH, H_2O, or LiOH within the synthesis, thus it is inevitable that H/OH will be present in "Li_3OCl". All may not be lost, however, after several experimental and computational studies show that a hydrated composition may be to the advantage of the ionic conductivity, as rotatable OH units enhance the mobility of Li-species in the bulk and at grain boundaries.[36–38] Ultimately this may come at a cost, as the conductivity has been shown to be highly

Department of Materials Science and Engineering, NTNU Norwegian University of Science and Technology, Trondheim, Norway. E-mail: benjamin.williamson@ntnu.no

† Electronic supplementary information (ESI) available. See DOI: https://doi.org/10.1039/d4ta08352k

This journal is © The Royal Society of Chemistry 2025

Open Access Article. Published on 18 February 2025. Downloaded on 2/20/2026 10:03:46 PM. This article is licensed under a Creative Commons Attribution 3.0 Unported Licence.

correlated with the proton and lithium vacancy concentration,[36] and controlling the amount of hydrogen in a hygroscopic material is difficult at best.[35] Whilst computational studies exist on the intrinsic defects of Li_3OCl,[30,33,39–42] including a full defect model by Squires *et al.*,[43] hydrogen has not previously been included in these. Squires *et al.* show that purely undoped Li_3OCl is an extended Schottky disordered material ($[V_{Li} + V_{Cl} + O_{Cl}]$), similar to what is seen in previously calculated models $[V_{Li} + V_{Cl}]$,[43] which Mouta *et al.* showed to enhance the ionic conductivity of Li_3OCl.[42] Squires also showed that undoped Li_3OCl could expect equilibrium ionic conductivities of $\sim 10^{-10}$ S cm^{-1}, significantly below experimental observations.[29]

Here, we present full intrinsic and extrinsic (H) defect models for metastable Li_3OCl, calculated with the hybrid functional HSE06. Using the quasi-harmonic approximation (QHA), the chemical potential stability region of Li_3OCl is shown to exist from ~750 K and shows that when undoped, Li_3OCl displays two types of Schottky disorder: full disorder under Li-rich conditions, and Li_2O disorder under Li-poor conditions. Hydrogen is shown to incorporate very easily, in line with the hygroscopic nature of Li_3OCl, and suppresses these Schottky defect clusters. Additionally, lithium substituted hydrogen is likely to relaxe offsite to form OH groups and induce a "pseudo-V_{Li}". Accounting for this defect in a conductivity model reproduces experimentally observed values.

2. Computational methods

Ab initio calculations were performed using DFT implemented within the plane-wave periodic code, VASP.[44–47] The projector-augmented wave method (PAW)[48,49] was used to describe the interaction between the core electrons and the valence electrons. All electrons were treated explicitly for Li, while for O, Cl, and H the standard pseudopotentials supplied with VASP were used. The hybrid functional HSE06 (Heyd–Scuseria–Ernzerhof)[50] was used in order to address the self-interaction error thus allowing for an accurate description of the band gap and electronic properties of Li_3OCl.

Hybrid functionals have consistently displayed improved geometry and electronic properties of semiconductors.[13,51–53] The band gap calculated herein is ~6.6 eV which aligns well with previous HSE06 studies (~6.4–6.6 eV).[43,53,54] To date, however, there is no experimental band gap with which to compare.

Determination of the bulk electronic and structural properties were performed on the cubic form (5 atom primitive cell) of Li_3OCl (space group: $Pm\bar{3}m$). To this end, a full geometric relaxation using a Γ-centred k-point grid of 6 × 6 × 6 and a plane wave energy cutoff of 500 eV was carried until the largest force on any atom was below the force criterion of 0.01 eV Å^{-1}. The intrinsic defects were simulated using a 3 × 3 × 3 supercell expansion of the conventional cell containing 135 atoms. Spin-polarised geometry relaxations (to the same convergence criteria as the conventional cell) of each defect cell and its respective charge states were performed using a Γ-centred 2 × 2 × 2 k-point mesh and 500 eV plane wave energy cutoff. A Γ-centred k-point 2 × 2 × 2 mesh was chosen in order to capture the M-point in the 1st Brillouin zone, which is the valence band maximum (VBM) and conduction band minimum (CBM) (ESI Fig. S1†), which was not captured in a Monkhorst–Pack 2 × 2 × 2 grid. The bulk electronic and structural properties are given in the ESI (Sections ESI 2 and ESI 1).†

2.1. Defect formalism

Eqn (1) describes the enthalpy of formation of a defect in charge state q:

$$\Delta H_f(D,q) = \left(E^{D,q} - E^{H}\right) + \sum_i n_i(\mu_i + \Delta\mu_i) + q\left(E_{Fermi} + \varepsilon^{H}_{VBM} + \Delta E^{pot}\right) + q^2 E^{IC}_{corr} + E^{BF}_{corr} \quad (1)$$

Where E^H is the total energy of the host supercell, $E^{D,q}$ is the total energy of the defective supercell in charge state q. Chemical potentials denoted by μ_i of each atomic species, i (Li(s), Cl_2(g), O_2(g), H_2(g)), are added to or removed from an external reservoir[55] by an amount n. In this work, the Fermi level ranges from the valence band maximum (VBM) at 0 eV (where ε^H_{VBM} denotes the eigenvalue of the VBM in the host material) to the conduction band minimum (CBM) which occurs at 6.38 eV. The potential of the defect supercell bar the immediate vicinity of the defect is averaged and aligned to the host supercell and is described by ΔE^{pot}.[56]

To account for the finite size effects of the defect supercells, two post-processing corrections are applied, E^{IC}_{corr} and E^{BF}_{corr}. The first correction term corresponds to the image-charge correction which minimises the long ranged nature of the Coulomb interaction[57,58] of the charged defect and its periodic images. The implementation used herein uses a formalism based upon the Lany and Zunger correction[56] with a 'non-cubic' adaptation as implemented by Hine and Murphy.[58,59] Lastly a band-filling correction is applied to shallow and resonant defects to account for the high carrier concentrations present in supercell calculations so as to regain the 'dilute limit'.[56,60]

2.2. Equilibrium concentrations

Equilibrium concentrations of defects in both Li_3OCl can be calculated self-consistently as implemented in the code `SC-FERMI`.[61] By determining the Fermi energy self-consistently the concentration of a defect D in charge state q can be evaluated through:

$$[D,q] = N_D g_{D,q} \exp\left(\frac{-\Delta H(D,q)}{kT}\right) \quad (2)$$

where N_D, $g_{D,q}$ and $\Delta H(D,q)$ are the number of sites on which the defect can form, the degeneracy of the defect state and the enthalpy of formation of the defect as calculated in eqn (1) respectively. Given a constraint of overall charge neutrality, the electron and hole concentrations can be determined from eqn (3) and (4):

$$n_0 = \int_{E_g}^{\infty} f_e(E)\rho(E)\mathrm{d}E \quad (3)$$

Open Access Article. Published on 18 February 2025. Downloaded on 2/20/2026 10:03:46 PM.
This article is licensed under a Creative Commons Attribution 3.0 Unported Licence.

$$p_0 = \int_{-\infty}^{0} f_h(E)\rho(E)\mathrm{d}E \quad (4)$$

where $\rho(E)$ is the density of states (DOS), E_g is the band gap and f_e is the Fermi–Dirac distribution function given by $f_e = \left[\exp\left(\frac{|E_F - E|}{kT}\right) + 1\right]^{-1}$ and $f_h = 1 - f_e(E)$. This approach has successful been applied to $Li_7La_3Zr_2O_{12}$ (ref. 13) (LLZO) and elsewhere.[51,62]

3. Results

3.1. Defining a chemical potential stability region for metastable Li_3OCl

Determination of the formation energies of defects in materials requires knowledge of the individual elemental chemical potentials (eqn (1)) which are typically constrained by the thermodynamic stability of the host material relative to competing phases. As Li_3OCl is metastable and not globally stable, calculating the chemical potentials requires either prior experimental knowledge about phase stability,[43] or calculation of host and competing phases at finite temperatures.[63] As the structure and composition of Li_3OCl is not widely acknowledged, the latter is chosen in this instance, however it is important to note that studies exist showing Li_3OCl to possess kinetic stability relative to LiCl and Li_2O,[30,64] proposed to be due to the sluggish anion transport in Li_3OCl.[65] In this study, the chemical potential limits analysis program (CPLAP[66]) is combined with the quasi-harmonic approximation (QHA) to determine the temperature dependent stability region of Li_3OCl and thus unveil suitable chemical potentials without *a priori* knowledge. This approach, whilst not widely used due to its increased computational expense, has shown recent success in determining the stability of $Na_2Ti_3O_7$.[63] From our results, Li_3OCl becomes the dominant phase at 750 K/476.85 °C (HSE06 functional), which agrees well with the expected experimental synthesis temperature from nominally non-hydrogen containing precursors, Li_2O and LiCl at (773 K/500 °C):[35]

$$Li_2O + LiCl \xrightarrow{500\,^\circ C} Li_3OCl \quad (5)$$

Typically, however, Li_3OCl is often formed *via* a solid state synthesis from a combination of LiCl and LiOH at lower temperatures:[27]

$$LiCl + 2LiOH \xrightarrow[\text{high vacuum, several days}]{330-360\,^\circ C} Li_3OCl + H_2O \quad (6)$$

An overview of the common synthesis routes is given in ESI Section 6† together with their calculated Gibbs free energy of reaction (ΔG_{reac}). Rettenwander and coworkers[35] showed that LiCl is still present after following the synthesis outlined in eqn (6) suggesting that Li_3OCl is Cl-poor. This indicates that OH^- is likely present in the samples due to an excess of LiOH.[35]

Nevertheless, a calculated stability region can be formed and is given in Fig. 1. What is seen is a very narrow region (straight line)

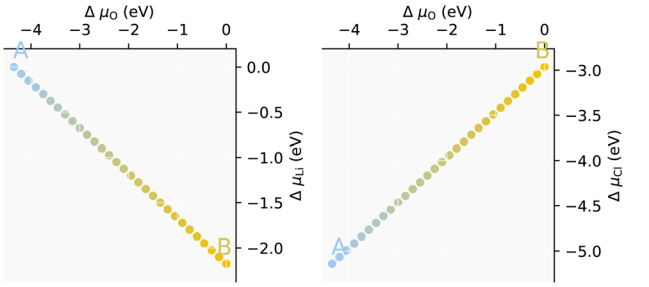

Fig. 1 The chemical potential limits of Li and Cl as a function of O chemical potential as calculated using HSE06 within the QHA formalism at 750 K. The chemical potential stability region is a thin area and is traversed by the coloured dots along μ_O from point A to point B.

between Li-rich/anion-poor ($\mu_{Li} = -2.17$ eV, $\mu_O = 0$ eV, $\mu_{Cl} = -2.97$ eV) designated point A, and Li-poor/anion-rich (($\mu_{Li} = 0$ eV, $\mu_O = -4.35$ eV, $\mu_{Cl} = -5.14$ eV)) designated point B. Whilst the results obtained from this method are somewhat strict, a larger region may be realised due to anion partial pressures. Anhydrous Li_3OCl can therefore be said to be stable over a more modest range of μ_{Li} than the larger μ_O and μ_{Cl}, anion deficiency or substitution in Li_3OCl is much more tolerated compared to Li deficiency, which could lead to thermodynamic instability towards other phases.

At point A, Li_3OCl is calculated to be in equilibrium with Li_2O, Li, and LiCl. At point B, Li_3OCl is in equilibrium with LiCl, Li_2O, and O_2.

3.2. Defect thermodynamics

The thermodynamic transition levels as calculated with the HSE06 functional for Li_3OCl are plotted in Fig. 2 showing both intrinsic (upper panels (a) and (b)) and extrinsic hydrogen defects (lower panels (c) and (d)) at anion-poor/Li-rich conditions (point A, in Fig. 1) and anion-rich/Li-poor conditions (point B in Fig. 1) respectively. Additionally, the equilibrium concentrations of the dominant defects ($\geq 1 \times 10^8$ cm^{-3}) are given in Fig. 3 as a function of oxygen chemical potential (μ_O) as one travels from point A to point B. Even though hydrogen incorporation is typically unavoidable in Li_3OCl we will still refer to it as "doping" for the case of simplicity in this work.

3.2.1 Intrinsic defects. The intrinsic defects of Li_3OCl are given in Fig. 2(a) and (b) for Li-rich and Li-poor conditions respectively. Equilibrium concentrations when undoped and under H-doping are given in Fig. 3(a) and (b) respectively. Under both regimes, lithium vacancies (V_{Li}) are the dominating defect possessing a formation energy of ~1.02 eV at the Fermi level (E_F ~ 3.71 eV and ~1.37 eV for Li-rich and Li-poor conditions respectively when undoped). If we compare the Fermi level calculated at $\mu_O = -1.08$ and -1.34 eV corresponding to the "experimentally accessible" oxygen chemical potentials of Li-rich and Li-poor conditions set out in the work by Squires *et al.*[43] we obtain formation energies of 2.05 eV and 1.89 eV respectively in good agreement with their values of ~2.20 eV and ~1.90 eV. A thermodynamic determination of the "experimentally accessible" region of oxygen chemical potentials is given in ESI Section 5.† Upon H-doping, E_F increases in energy to ~4.12 eV and ~1.72 eV for Li-rich and Li-poor conditions

 This journal is © The Royal Society of Chemistry 2025

Open Access Article. Published on 18 February 2025. Downloaded on 2/20/2026 10:03:46 PM.
This article is licensed under a Creative Commons Attribution 3.0 Unported Licence.

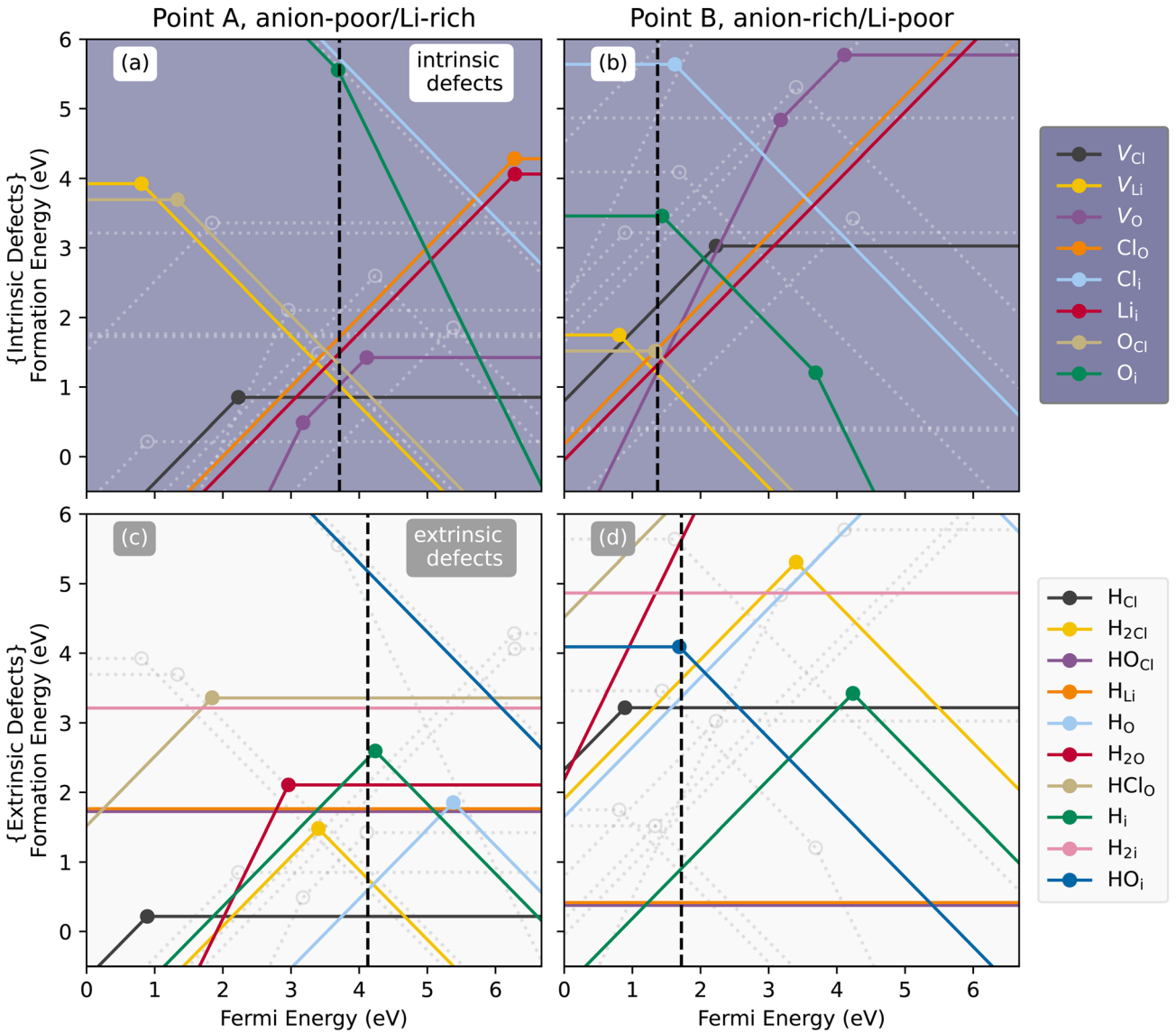

Fig. 2 The thermodynamic transition levels for (a) and (b) intrinsic defects and (c) and (d) extrinsic H defects for the chemical potentials at points A (O-poor) and B (O-rich) respectively at 750 K, 1 atm. In each example the dashed vertical line represents the equilibrium Fermi level (E_F) and the corresponding extrinsic and intrinsic defects are shown by the faded dotted lines for reference.

respectively. Pushing E_F higher in energy, such as through doping[43] results in an ease in the formation of V_{Li}, increasing the concentration and therefore the ionic conductivity.

3.2.2 Li-rich/anion-poor conditions, point A. The dominant intrinsic defects are seen to be V_{Li}, V_{Cl}, and V_O, indicative of full Schottky disorder. This is partially in agreement with previous literature findings[30,39,42,43] where three types of Schottky disorder are predicted, either "LiCl" partial Schottky: (V_{Li} + V_{Cl}), Li_2O partial Schottky: ($2V_{Li}$ + V_O) or in the case of Squires *et al.*: (V_{Li} + V_{Cl} + O_{Cl}) (under Li-rich conditions).[39,42,43] Contrary to Squires *et al.*, however, in this work, both antisite defects, O_{Cl} and Cl_O, whilst forming in modest quantities, ($\sim 10^{12}$–10^{13} cm^{-3}) are not expected to dominate the defect landscape of Li_3OCl. It is important to note that, O_{Cl} does increase to concentrations $\geq 10^{16}$ cm^{-3} upon H-doping, as seen in Fig. 3(b) simultaneously reducing [V_O], thus it could be said that the modified Schottky defect as calculated by Squires *et al.*[43] is somewhat valid. The full Schottky defect calculated in this work is interesting in that V_{Cl} and V_O exist in the neutral ($q = 0$) and partially ionised ($q = 1+$) charge states respectively. Charge neutrality of the defect cluster is consequently caused by V_{Li} and V_O and can be defined in Kröger–Vink form as:

$$4Li_{Li}^{\times} + 4O_O^{\times} + 2Cl_{Cl}^{\times} \rightarrow 4V_{Li}^{'} + 4V_O^{\cdot} + 2V_{Cl}^{\times} + 2Li_2O + O_2 + Cl_2 \quad (7)$$

Partial charge densities are provided in ESI Fig. S5–S7† for V_{Li}, V_O, and V_{Cl} and their corresponding charge states,

Open Access Article. Published on 18 February 2025. Downloaded on 2/20/2026 10:03:46 PM.
This article is licensed under a Creative Commons Attribution 3.0 Unported Licence.

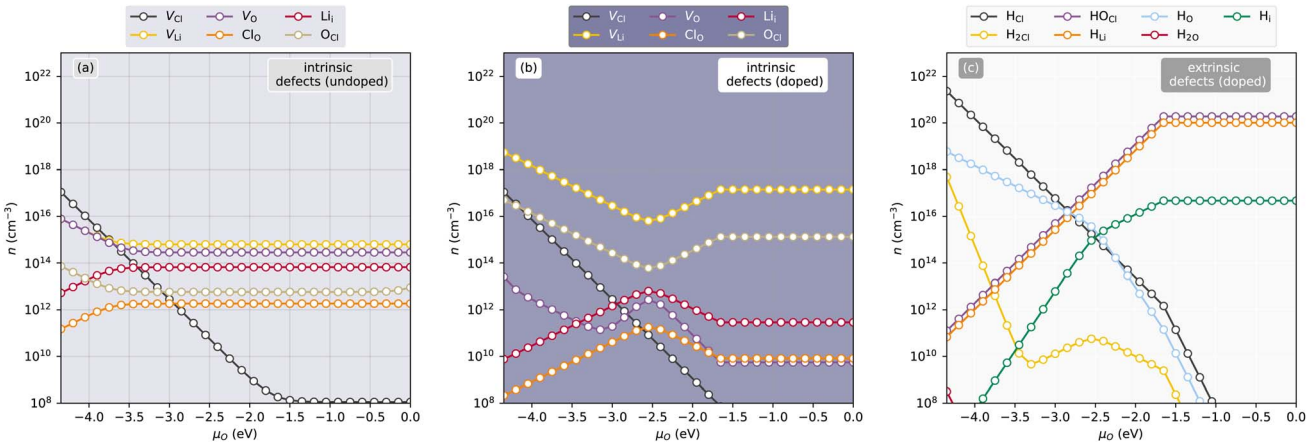

Fig. 3 The equilibrium concentrations of all defects within Li_3OCl as a function of oxygen chemical potential, μ_O, (indicating the change from anion poor to anion rich conditions) with concentrations > $\times 10^5$ cm^{-3} as calculated at 750 K/1 atm. (a) Shows the undoped intrinsic defect concentrations, whilst (b) and (c) show the intrinsic and extrinsic H-doped defect concentrations respectively.

respectively. What results are localised electrons within the anion vacancies and a localised hole on an adjacent O 2p orbital for V_{Li}. Such localizations induce slight local structure distortions around the defect, which can enhance the mobility of Li.[12] As observed in the undoped concentrations in Fig. 3(a), [V_{Cl}] decreases rapidly between point A (anion poor) and point B (anion rich), and is not wholly influenced by H. This is in contrast to what is seen in Squires *et al.* where they show that the LiCl Schottky defect (V_{Li} + V_{Cl}) is predicted.

3.2.3 Li-poor/anion-rich conditions, point B. V_{Li} and V_O dominate under these conditions and in the transition level diagram in Fig. 2(b) it can be seen that V_O rises in energy such that it is in the 2+ charge state at E_F. The full Schottky defect in eqn (7) at Li-rich conditions, thus becomes ($2V_{Li}$ + V_O). In previous literature, this has been described as the Li_2O Schottky defect:[39,42]

$$2Li_{Li}^{\times} + O_O^{\times} \rightarrow 2V_{Li}^{'} + V_O^{\cdot\cdot} + Li_2O \quad (8)$$

Counterintuitively, equilibrium [V_{Li}] under Li-rich conditions are higher than those under Li-poor conditions ($\sim 8 \times 10^{15}$ cm^{-3} *vs.* $\sim 6 \times 10^{14}$ cm^{-3}) despite the existence of neutral V_{Cl} under Li-rich conditions. Incidentally, interstitial Li (Li_i) will not be the dominant charge carrier over the entirety of the chemical potential range, which is echoed by previous literature,[29] despite its lower migration barrier.[30] ESI Fig. S8† shows the partial charge density of Li_i showing distinct local distortion due to sterics, but delocalised electron density allowing for reduced coulombic repulsion which likely supports the lower migration barrier. Despite this, it is expected that Li_i will be present, albeit in small quantities in undoped Li_3OCl ($\sim 7 \times 10^{13}$ cm^{-3}) in a combined Schottky–Frenkel defect:

$$3Li_{Li}^{\times} + O_O^{\times} + V_i^{\times} \rightarrow 3V_{Li}^{'} + V_O^{\cdot\cdot} + Li_i^{\cdot} + Li_2O \quad (9)$$

Upon H-doping, however, Li_i and V_O become suppressed as evident in Fig. 3(b) severely reducing both Li_2O Schottky and Schottky–Frenkel disorder under Li-poor conditions in Li_3OCl.

3.2.4 Extrinsic hydrogen defects. In this study, H-doping involving H, H_2, OH, and HCl defects are considered. The formation energies under Li-rich/anion-poor and Li-poor/anion-rich conditions are given in Fig. 2(c) and (d) respectively, and equilibrium defect concentrations in Fig. 3(c). In general, HCl and H_2 defects are high in energy and are not preferential to form, thus the thermodynamically favourable H-species are OH and singular H defects. This is in line with experimental suggestions that Li_3OCl is Cl-poor and OH rich.[35]

3.2.5 Li-rich/anion-poor conditions, point A. The dominant H-defect is neutral H_{Cl} possessing a formation energy of $\sim$0.22 eV at E_F. This results in an equilibrium concentration of $\sim 2 \times 10^{21}$ cm^{-3}. As previously stated, E_F is shifted further away from the VBM in the band gap from 3.71 eV to 4.13 eV upon H-incorporation. This has an additional role in lowering the cost of formation of V_{Li} from $\sim$1.02 eV to $\sim$0.60 eV thereby increasing its equilibrium concentration from $\sim 8 \times 10^{15}$ cm^{-3} to $\sim 5 \times 10^{18}$ cm^{-3}. The next dominant hydrogen defect under Li-rich conditions is H_O. H_O forms at $\sim$0.60 eV at E_F, resulting in a concentration of $\sim 6 \times 10^{18}$ cm^{-3}. Whilst H_{Cl} dominates at these conditions, it is H_O in the 1+ charge state that compensates V_{Li}. This results in a diminished [V_O] compared to undoped Li_3OCl, and thus destruction of the full Schottky disorder as explained in eqn (7). Towards Li-poor conditions both these defects tail off in favour of H_{Li} and OH_{Cl}, both neutral defects in themselves at $\mu_O = \sim -2.8$ eV. It is expected, therefore that unintentional H-doping at these conditions results in an expected increase in mobile V_{Li} and thus ionic conductivity. [Li_i] is reduced upon H-doping from $\sim 5 \times 10^{12}$ cm^{-3} to $\sim 8 \times 10^9$ cm^{-3}. Under Li-rich conditions, the defect chemistry can be expressed as:

$$3H_2 + 4Li_{Li}^{\times} + 4O_O^{\times} + 2Cl_{Cl}^{\times} \rightarrow 4V_{Li}^{'} + 4H_O^{\cdot} + 2H_{Cl}^{\times} + 2Li_2O + O_2 + Cl_2 \quad (10)$$

3.2.6 Li-poor/anion-rich conditions, point B. H_{Li} and HO_{Cl} quickly become the dominant species with formation energies

 This journal is © The Royal Society of Chemistry 2025

Open Access Article. Published on 18 February 2025. Downloaded on 2/20/2026 10:03:46 PM. This article is licensed under a Creative Commons Attribution 3.0 Unported Licence.

at E_F under point B of around 0.42 and 0.37 eV respectively. As both defects are neutral ($q = 0$), they aren't expected to be charge compensated by any intrinsic or otherwise H-related species. The equilibrium concentrations of [H_{Li}] and [HO_{Cl}] are fairly high $\sim 1 \times 10^{20}$ cm^{-3} and $\sim 2 \times 10^{20}$ cm^{-3} respectively. It is important to note, that whilst "equilibrium concentrations" are stated, we are constrained by the formation of Li_3OCl and it is highly likely that in reality excess H will make its way into the structure increasing H defect concentrations, or form additional $Li_{3-x}OH_xCl$ phases or Li_2OHCl. Upon H doping under Li-poor conditions, E_F again, shifts towards the conduction band minimum (CBM) from 1.37 eV to 1.7 eV resulting in a lower effective formation energy of V_{Li} from $\sim$1.18 eV to $\sim$0.84 eV. As at point A, it is expected that [V_{Li}] rises from $\sim 6 \times 10^{14}$ cm^{-3} when undoped to $\sim 1.4 \times 10^{17}$ cm^{-3}.

Fig. 4(a) and (b) show the relaxed defect supercells of HO_{Cl} (at $q = 0$), and H_{Li} (at $q = 0$) respectively. HO_{Cl}, warps the structure shifting adjacent Li away from its preferred site (Wyckoff: 3c) towards the neutral cluster. As this defect is nominally neutral, the displacement arises due to the smaller OH^- radii (110 pm) compared to Cl^- radii (181 pm) and may aid in improving Li-ion transport by increasing "accessible space" and weakening the Li–O bonds. In H_{Li} (Fig. 4(b)), H shifts off its Li site (3c) towards an adjacent O forming a neutral OH. This defect can therefore be seen as a "pseudo-V_{Li}" or as suggested by Song *et al.*[67] a Frenkel-type defect as any moving Li into this space technically becomes an interstitial. Experimentally, Schwering *et al.*[68] suggested H_{Li} as the dominant defect, remarking also that H_{Li} provides rotatable OH that facilitates Li transport. Work carried out by Eilbracht *et al.*[69] using single crystal data on Li_2OHCl also suggest Li site occupation. Similar evaluations of the role of rotatable OH groups have been suggested in the literature.[36,67,70] Dawson *et al.*[36] using molecular dynamics simulations (MD) combined with ^{2}H NMR spectroscopy, observe that both highly rotatable OH groups exist alongside fixed OH groups. Further investigation shows that OH rotations are more free when O is coordinated to fewer lithiums.

4. Discussion

In this study, we have performed hybrid functional charged defect calculations on H-doped Li_3OCl. This is in order to determine the influence of hydrogen on intrinsic defect chemistry of Li_3OCl and its influence on structure and ionic conductivity. In this model we have considered all vacancies, interstitials, antisites and varying H-related extrinsic species such as singular H, H_2, OH and HCl. A self-consistent model such as this is highly important for getting a holistic overview of the mechanisms for ionic conductivity as well unravelling the thermodynamics of Li_3OCl as given in experimental and computational studies in previous literature.[30,33,36,39–42,67,70]

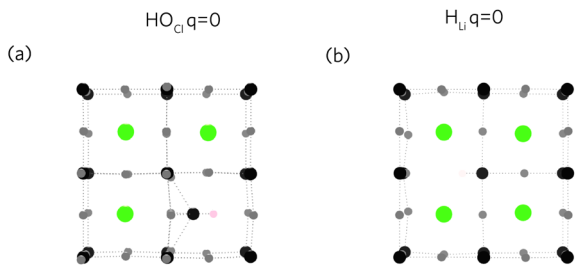

Fig. 4 Relaxed defect structures of (a) HO_{Cl} ($q = 0$), and (b) H_{Li} ($q = 0$). In each example, lithium is coloured grey, chlorine is green, oxygen is black and hydrogen is pink. In (b), H_{Li} relaxes towards O forming a neutral OH species and forming a pseudo-V_{Li}.

Taking undoped Li_3OCl, we find that across the range of synthesis conditions, (Li-poor to Li-rich), V_{Li} is the dominant charge carrying defect whilst Li_i exists in much lower concentrations, thus ruling out an interstitial or interstitialcy mechanism within Li_3OCl consistent with other reports,[30,42,43,71] despite the lower migration energy barrier of 0.17 eV (compared to 0.34 eV for V_{Li}).[30] Under the most Li-rich/anion-poor conditions, the full Schottky defect exists, (V_{Li} + V_O + V_{Cl}), however with V_{Cl} existing in the neutral charge state. This is somewhat contrary to previous reports of Li_3OCl being LiCl ([V_{Li} + V_{Cl}]) Schottky disordered.[30,40,43,72,73] It is important to note, however, that with the exception of the work in ref. 43, the other studies only consider neutral defects and assume full charge neutrality from V_{Li} and V_{Cl}, yet we find that the positive compensating defect for V_{Li} are oxygen vacancies (V_O). This changes to a Li_2O Schottky defect (V_{Li} + V_O) under Li-poor conditions. Equally, whilst antisites are expected to form in small quantities ($\sim 10^{12}$–10^{13} cm^{-3}) in undoped Li_3OCl, our results do not point towards significant anion disorder.[18] Consensus in the literature is that anion disorder is beneficial to increasing the conductivity of Li-ion solid electrolytes. This is attributed to significant anion disorder opening up percolating three-dimensional pathways previously inaccessible to anion ordered systems.[15] In a paper by Li *et al.*[74] they stated that due to the size mismatch between O and Cl, anion antisite defects would cause a strong structural distortion and an electrostatic penalty for mobile lithium defects thus reducing the conductivity.

The inconsistency between this work and previous calculations is likely down to both the choice of functional, as well as from the calculation of the chemical potential stability region for Li_3OCl of which the defect formation energies are highly sensitive to. Hybrid functionals typically give a much better description of electron localisation for defects, as well as favourable description of the band gap of a material relative to experiment.[12,52,75,76] Both of these are crucial when determining charged defect calculations in order to correctly describe the thermodynamic defect quantities of solid electrolytes.[12,13,18,43] In this work, the chemical potential region was determined "temperature-dependently" through calculating the free energies of competing phases using QHA (Section 3 3.1), which has shown success previously in $Na_2Ti_3O_7$.[63] Confidence in this result arises from the fact that Li_3OCl becomes "stable" around $\sim$750 K, in excellent agreement with the experimental synthesis temperature (without H) of $\sim$773 K.[35]

The unfortunate reality of Li_3OCl is that it is highly unlikely to be purely Li_3OCl, but a hydrated form $Li_{3-x}OH_xCl$.[35,36] Even when attempting to create dehydrated forms of Li_3OCl, Li *et al.*[77] acknowledged that some form of OH is observable from FTIR. This work shows that hydrogen defects are omnipresent in the

Open Access Article. Published on 18 February 2025. Downloaded on 2/20/2026 10:03:46 PM. This article is licensed under a Creative Commons Attribution 3.0 Unported Licence.

structure of Li_3OCl and high defect concentrations of at least $\geq 10^{20}$ cm^{-3} are to be expected. Our results indicate a baseline equilibrium which is likely to be higher based on both synthesis conditions and local atmosphere indeed forming Li_2OHCl. Nevertheless, our results do not rule out the formation of cubic anti-perovskite Li_3OCl without forming full Li_2OHCl compositions. Dawson *et al.* showed that hydrogen does not diffuse in Li_3OCl due to the large jump distances of 3.91 Å.[36]

Under Li-rich conditions, it is expected that neutral H_{Cl} forms as the dominant defect which pushes E_F higher in energy towards the CBM thereby reducing the formation energy of V_{Li} within the crystal structure. Additionally in work carried out by Gao *et al.*,[37,78] they showed that in M_3HCh (M = Li, Na; Ch = S, Se, Te), that the influence of H^- reduced the energy barrier of migration due to its large polarizability, thus a similar effect may be present here with H_{Cl}. At the same time, H-incorporation suppresses the Schottky disorder as seen in purely undoped Li_3OCl. This is also the case under Li-poor conditions, whereby the Li_2O Schottky disorder is cancelled by the neutral hydrogen defects: H_{Li} and OH_{Cl}. H_{Li} is seen to relax off its nominal Li site towards an adjacent oxygen forming an "OH_O" which can also be seen as a "pseudo-V_{Li}". Work by Schwering *et al.*[68] on Li_3OCl and Eilbracht *et al.*[69] on Li_2OHCl agree with this conclusion. This "pseudo-V_{Li}" can also be seen as a Frenkel defect, where the mobile Li becomes effectively an interstitial upon rotation of the OH species.[67] Additionally, OH_{Cl}, whilst neutral, acts to distort the structure slightly due to its smaller radii compared to Cl which may also aid Li mobility.

Squires *et al.*[43] calculated the conductivity of Li_3OCl within their full defect model through:

$$\sigma = \frac{Cq^2}{kT} D^* \quad (11)$$

where C is the concentration of mobile ions, q is the charge of those ions, k the Boltzmann constant, T the temperature and the self-diffusion coefficient is given by D^* and takes into account the attempt frequency (1×10^{13} Hz), the hop distance (2.67 Å (ref. 43)) and the migration barrier, E_m (0.34 eV (ref. 30)).[43] In their work they showed that undoped Li_3OCl expects values of $\sim 10^{-10}$ S cm^{-1} far off the values present in experiment ($\sim 10^{-6}$–10^{-2} S cm^{-1}).[29]

Fig. 5 displays the ionic conductivity as a function of μ_O calculated with the same strategy using our defect model for undoped and H-doped Li_3OCl. Our results align well with Squires *et al.*[43] where low conductivities of $\sim 10^{-10}$ S cm^{-1} are observed. Upon incorporation of hydrogen, the V_{Li} conductivity increases from $\sim 3.75 \times 10^{-11}$ S cm^{-1} under Li-poor conditions to $\sim 3.35 \times 10^{-10}$ S cm^{-1} under Li-rich conditions. By including the "pseudo-V_{Li}" into our model, before considering potential enhancements to the mobility due to OH rotations the ionic conductivity of H-doped Li_3OCl lie in the region of $\sim 10^{-6}$ S cm^{-1} in better agreement with experiment. Work by Dawson *et al.*[36] showed that lower concentrations of H within Li_3OCl resulted in lower migration energy barriers ~0.30 eV whilst Song *et al.*[67] predicted values of ~0.24/0.26 eV. Whilst OH_{Cl} has an increased Li-coordination to H_{Li}, it is likely that

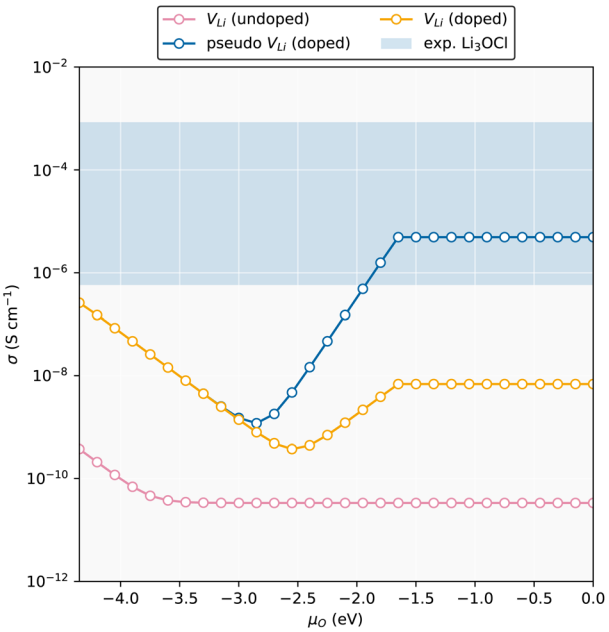

Fig. 5 Room temperature ionic conductivity as a function of oxygen chemical potential taking into account the sum of V_{Li} and Li_i. Included is also the "pseudo" V_{Li} whereby H_{Li} is treated as a V_{Li} using the same migration barrier. The blue shaded region corresponds to experimental conductivities taken from ref. 27 and 79.

OH_{Cl} may lower the barrier for migration in a similar way that Br does in $Li_3OCl_{1-n}Br_n$.[80]

5. Conclusions

In this work we illustrate the need for consideration of hydrogen as both a compositional changing opportunistic dopant, as well as a strategy for enhancing the ionic conductivity, not only in Li_3OCl but other hygroscopic solid electrolytes as well. A full defect model combined with a temperature dependent defined chemical potential stability region is necessary in order to outline doping strategies, killer defects, as well as structural changes in a given material. Our results highlight that, when undoped, Li_3OCl can expect a degree of Schottky disorder, both full and Li_2O-Schottky, in line with other computational predictions. Such a disorder, particularly anion disorder, can give rise to favourable ionic mobility of Li-species within the structure, similar to that in other solid electrolytes. Upon inevitable hydrogen incorporation, the Schottky disorder disappears, instead favouring the formation of neutral H species such as OH_{Cl} and H_{Li}. H_{Li} is shown to relax off site towards an adjacent oxygen forming an effective (OH_O + V_{Li}) defect pair, or a "pseudo-V_{Li}". Considering only purely V_{Li} results in low ionic conductivities, however, upon consideration of a "pseudo-V_{Li}", our calculated ionic conductivities are more in line with experimentally observed values. Whilst Li_3OCl remains a controversial and challenging material, our results show that H may be a source of enhancement in Li_3OCl, increasing both the ionic mobility due to OH rotations, as well as increasing the effective carrier concentration.

This journal is © The Royal Society of Chemistry 2025

Open Access Article. Published on 18 February 2025. Downloaded on 2/20/2026 10:03:46 PM. This article is licensed under a Creative Commons Attribution 3.0 Unported Licence.

Data availability

The data for this article have been included as part of the ESI.†

Author contributions

BADW provided the idea for this study and performed the calculations and analysis, with help from KE. BADW wrote the manuscript, and all authors contributed to the reviewing and editing of the final manuscript and have given approval to the final version of the manuscript. SMS provided funding for this project.

Conflicts of interest

There are no conflicts of interest in this work.

Acknowledgements

This work was supported by the Research Council of Norway through Projects no. 275810 and 302506. Computational resources were provided by UNINETT Sigma2 through Projects NN9264K and ntnu243. B.A.D.W would like to acknowledge Nora S. Løndal and Caren R. Zeiger for useful discussions.

References

1 T. Kim, W. Song, D.-Y. Son, L. K. Ono and Y. Qi, *J. Mater. Chem. A*, 2019, **7**, 2942.
2 K. Mizushima, P. C. Jones, P. J. Wiseman and J. B. Goodenough, *Mater. Res. Bull.*, 1980, **15**, 783.
3 S. Geller and J. L. Durand, *Acta Crystallogr.*, 1960, **13**, 325.
4 J. Li and Z.-F. Ma, *Chem*, 2019, **5**, 3.
5 H.-J. Noh, S. Youn, C. S. Yoon and Y.-K. Sun, *J. Power Sources*, 2013, **233**, 121.
6 Z. Huang, Z. Xiao, R. Jin, Z. Li, C. Shu, R. Shi, X. Wang, Z. Tang, W. Tang and Y. Wu, *Energy Environ. Sci.*, 2024, **17**, 5365.
7 D. Lu, Y. Shao, T. Lozano, W. D. Bennett, G. L. Graff, B. Polzin, J. Zhang, M. H. Engelhard, N. T. Saenz, W. A. Henderson, P. Bhattacharya, J. Liu and J. Xiao, *Adv. Energy Mater.*, 2015, **5**, 1400993.
8 J. Janek and W. G. Zeier, *Nat. Energy*, 2016, **1**, 1.
9 X. Fan and C. Wang, *Chem. Soc. Rev.*, 2021, **50**, 10486.
10 S. S. Park, S. A. Han, R. Chaudhary, J. H. Suh, J. Moon, M.-S. Park and J. H. Kim, *Adv. Energy Sustainability Res.*, 2023, **4**, 2300074.
11 I. T. Røe, S. M. Selbach and S. K. Schnell, *J. Phys. Chem. Lett.*, 2020, **11**, 2891.
12 K. Eggestad, S. M. Selbach and B. A. D. Williamson, *J. Mater. Chem. A*, 2024, **12**, 15666–15675.
13 A. G. Squires, D. O. Scanlon and B. J. Morgan, *Chem. Mater.*, 2020, **32**, 1876.
14 A. G. Squires, D. W. Davies, S. Kim, D. O. Scanlon, A. Walsh and B. J. Morgan, *Phys. Rev. Mater.*, 2022, **6**, 085401.
15 B. J. Morgan, *Chem. Mater.*, 2021, **33**, 2004.
16 M. A. Kraft, S. P. Culver, M. Calderon, F. Böcher, T. Krauskopf, A. Senyshyn, C. Dietrich, A. Zevalkink, J. Janek and W. G. Zeier, *J. Am. Chem. Soc.*, 2017, **139**, 10909.
17 C. Yu, F. Zhao, J. Luo, L. Zhang and X. Sun, *Nano Energy*, 2021, **83**, 105858.
18 P. Gorai, H. Long, E. Jones, S. Santhanagopalan and V. Stevanović, *J. Mater. Chem. A*, 2020, **8**, 3851.
19 S. P. Ong, Y. Mo, W. D. Richards, L. Miara, H. S. Lee and G. Ceder, *Energy Environ. Sci.*, 2012, **6**, 148.
20 N. Kamaya, K. Homma, Y. Yamakawa, M. Hirayama, R. Kanno, M. Yonemura, T. Kamiyama, Y. Kato, S. Hama, K. Kawamoto and A. Mitsui, *Nat. Mater.*, 2011, **10**, 682.
21 V. Lacivita, A. S. Westover, A. Kercher, N. D. Phillip, G. Yang, G. Veith, G. Ceder and N. J. Dudney, *J. Am. Chem. Soc.*, 2018, **140**, 11029.
22 P. López-Aranguren, M. Reynaud, P. Głuchowski, A. Bustinza, M. Galceran, J. M. López del Amo, M. Armand and M. Casas-Cabanas, *ACS Energy Lett.*, 2021, **6**, 445.
23 F. Han, A. S. Westover, J. Yue, X. Fan, F. Wang, M. Chi, D. N. Leonard, N. J. Dudney, H. Wang and C. Wang, *Nat. Energy*, 2019, **4**, 187.
24 S. Nowak, F. Berkemeier and G. Schmitz, *J. Power Sources*, 2015, **275**, 144.
25 Z. Zhang, Y. Shao, B. Lotsch, Y.-S. Hu, H. Li, J. Janek, L. F. Nazar, C.-W. Nan, J. Maier, M. Armand and L. Chen, *Energy Environ. Sci.*, 2018, **11**, 1945.
26 S. Zhang, J. Ma, S. Dong and G. Cui, *Electrochem. Energy Rev.*, 2023, **6**, 4.
27 Y. Zhao and L. L. Daemen, *J. Am. Chem. Soc.*, 2012, **134**, 15042.
28 X. Lü, J. W. Howard, A. Chen, J. Zhu, S. Li, G. Wu, P. Dowden, H. Xu, Y. Zhao and Q. Jia, *Adv. Sci.*, 2016, **3**, 1500359.
29 J. A. Dawson, T. Famprikis and K. E. Johnston, *J. Mater. Chem. A*, 2021, **9**, 18746.
30 A. Emly, E. Kioupakis and A. Van der Ven, *Chem. Mater.*, 2013, **25**, 4663.
31 T. H. Wan, Z. Lu and F. Ciucci, *J. Power Sources*, 2018, **390**, 61.
32 K. Hippler, S. Sitta, P. Vogt and H. Sabrowsky, *Acta Crystallogr., Sect. C*, 1990, **46**, 736.
33 Z. Wang and G. Shao, *J. Mater. Chem. A*, 2017, **5**, 21846.
34 S. Gao, T. Broux, S. Fujii, C. Tassel, K. Yamamoto, Y. Xiao, I. Oikawa, H. Takamura, H. Ubukata, Y. Watanabe, K. Fujii, M. Yashima, A. Kuwabara, Y. Uchimoto and H. Kageyama, *Nat. Commun.*, 2021, **12**, 201.
35 I. Hanghofer, G. J. Redhammer, S. Rohde, I. Hanzu, A. Senyshyn, H. M. R. Wilkening and D. Rettenwander, *Chem. Mater.*, 2018, **30**, 8134.
36 J. A. Dawson, T. S. Attari, H. Chen, S. P. Emge, K. E. Johnston and M. S. Islam, *Energy Environ. Sci.*, 2018, **11**, 2993.
37 A. C. C. Dutra and J. A. Dawson, *J. Phys. Chem. C*, 2023, **127**, 18256.
38 J. A. Quirk and J. A. Dawson, *Adv. Energy Mater.*, 2023, **13**, 2301114.
39 Z. Lu, C. Chen, Z. M. Baiyee, X. Chen, C. Niu and F. Ciucci, *Phys. Chem. Chem. Phys.*, 2015, **17**, 32547.

Open Access Article. Published on 18 February 2025. Downloaded on 2/20/2026 10:03:46 PM. This article is licensed under a Creative Commons Attribution 3.0 Unported Licence.

40 A. Baktash, B. Demir, Q. Yuan and D. J. Searles, *Energy Storage Mater.*, 2021, **41**, 614.
41 Z. Zhang, Z. Ma and Y. Pei, *Phys. Chem. Chem. Phys.*, 2023, **25**, 13297.
42 R. Mouta, M. A. B. Melo, E. M. Diniz and C. W. A. Paschoal, *Chem. Mater.*, 2014, **26**, 7137.
43 A. G. Squires, J. M. Dean and B. J. Morgan, *Chemrxiv*, 2021, preprint, DOI: 10.26434/chemrxiv-2021-hzrls.
44 G. Kresse and J. Hafner, *Phys. Rev. B:Condens. Matter Mater. Phys.*, 1994, **49**, 14251.
45 G. Kresse and J. Hafner, *Phys. Rev. B:Condens. Matter Mater. Phys.*, 1993, **47**, 558.
46 G. Kresse and J. Furthmüller, *Comput. Mater. Sci.*, 1996, **6**, 15.
47 G. Kresse and J. Furthmüller, *Phys. Rev. B:Condens. Matter Mater. Phys.*, 1996, **54**, 11169.
48 P. E. Blöchl, *Phys. Rev. B:Condens. Matter Mater. Phys.*, 1994, **50**, 17953.
49 G. Kresse and D. Joubert, *Phys. Rev. B:Condens. Matter Mater. Phys.*, 1999, **59**, 1758.
50 A. V. Krukau, O. A. Vydrov, A. F. Izmaylov and G. E. Scuseria, *J. Chem. Phys.*, 2006, **125**, 224106.
51 B. A. D. Williamson, J. Buckeridge, N. P. Chadwick, S. Sathasivam, C. J. Carmalt, I. P. Parkin and D. O. Scanlon, *Chem. Mater.*, 2019, **31**, 2577.
52 B. A. D. Williamson, T. J. Featherstone, S. S. Sathasivam, J. E. N. Swallow, H. Shiel, L. A. H. Jones, M. J. Smiles, A. Regoutz, T.-L. Lee, X. Xia, C. Blackman, P. K. Thakur, C. J. Carmalt, I. P. Parkin, T. D. Veal and D. O. Scanlon, *Chem. Mater.*, 2020, **32**, 1964.
53 M. Wu, B. Xu, X. Lei, K. Huang and C. Ouyang, *J. Mater. Chem. A*, 2018, **6**, 1150.
54 Y. Zhang, Y. Zhao and C. Chen, *Phys. Rev. B:Condens. Matter Mater. Phys.*, 2013, **87**, 134303.
55 C. G. Van de Walle and J. Neugebauer, *J. Appl. Phys.*, 2004, **95**, 3851.
56 S. Lany and A. Zunger, *Phys. Rev. B:Condens. Matter Mater. Phys.*, 2008, **78**, 235104.
57 R. M. Nieminen, *Model. Simul. Mater. Sci. Eng.*, 2009, **17**, 084001.
58 N. D. M. Hine, K. Frensch, W. M. C. Foulkes and M. W. Finnis, *Phys. Rev. B:Condens. Matter Mater. Phys.*, 2009, **79**, 024112.
59 S. T. Murphy and N. D. M. Hine, *Phys. Rev. B:Condens. Matter Mater. Phys.*, 2013, **87**, 094111.
60 C. Persson, Y.-J. Zhao, S. Lany and A. Zunger, *Phys. Rev. B:Condens. Matter Mater. Phys.*, 2005, **72**, 035211.
61 J. Buckeridge, *Comput. Phys. Commun.*, 2019, **244**, 329.
62 F. H. Taylor, J. Buckeridge and C. R. A. Catlow, *Chem. Mater.*, 2016, **28**, 8210.
63 Y.-S. Choi, S. I. R. Costa, N. Tapia-Ruiz and D. O. Scanlon, *ACS Appl. Energy Mater.*, 2023, **6**, 484.
64 M.-H. Chen, A. Emly and A. Van der Ven, *Phys. Rev. B:Condens. Matter Mater. Phys.*, 2015, **91**, 214306.
65 J. a. S. Serejo, J. S. Pereira, R. Mouta and L. G. C. Rego, *Phys. Chem. Chem. Phys.*, 2021, **23**, 6964.
66 J. Buckeridge, D. O. Scanlon, A. Walsh and C. R. A. Catlow, *Comput. Phys. Commun.*, 2014, **185**, 330.
67 A.-Y. Song, Y. Xiao, K. Turcheniuk, P. Upadhya, A. Ramanujapuram, J. Benson, A. Magasinski, M. Olguin, L. Meda, O. Borodin and G. Yushin, *Adv. Energy Mater.*, 2018, **8**, 1700971.
68 G. Schwering, A. Hönnerscheid, L. van Wüllen and M. Jansen, *ChemPhysChem*, 2003, **4**, 343.
69 C. Eilbracht, W. Kockelmann, D. Hohlwein and H. Jacobs, *Physica B*, 1997, **234**, 48.
70 F. Wang, H. A. Evans, K. Kim, L. Yin, Y. Li, P.-C. Tsai, J. Liu, S. H. Lapidus, C. M. Brown, D. J. Siegel and Y.-M. Chiang, *Chem. Mater.*, 2020, **32**, 8481.
71 X. Lü, J. W. Howard, A. Chen, J. Zhu, S. Li, G. Wu, P. Dowden, H. Xu, Y. Zhao and Q. Jia, *Adv. Sci.*, 2016, **3**, 1500359.
72 Y. Zhang, X. He, Z. Chen, Q. Bai, A. M. Nolan, C. A. Roberts, D. Banerjee, T. Matsunaga, Y. Mo and C. Ling, *Nat. Commun.*, 2019, **10**, 5260.
73 J. A. Dawson, H. Chen and M. S. Islam, *J. Phys. Chem. C*, 2018, **122**, 23978.
74 P. Li, F. Hussain, P. Cui, Z. Li and J. Yang, *Phys. Rev. Mater.*, 2019, **3**, 115402.
75 D. Broberg, K. Bystrom, S. Srivastava, D. Dahliah, B. A. D. Williamson, L. Weston, D. O. Scanlon, G.-M. Rignanese, S. Dwaraknath, J. Varley, K. A. Persson, M. Asta and G. Hautier, *npj Comput. Mater.*, 2023, **9**, 1.
76 M. Quesada-Gonzalez, B. A. D. Williamson, C. Sotelo-Vazquez, A. Kafizas, N. D. Boscher, R. Quesada-Cabrera, D. O. Scanlon, C. J. Carmalt and I. P. Parkin, *J. Phys. Chem. C*, 2018, **122**, 714.
77 Y. Li, W. Zhou, S. Xin, S. Li, J. Zhu, X. Lü, Z. Cui, Q. Jia, J. Zhou, Y. Zhao and J. B. Goodenough, *Angew. Chem., Int. Ed.*, 2016, **55**, 9965.
78 S. Gao, T. Broux, S. Fujii, C. Tassel, K. Yamamoto, Y. Xiao, I. Oikawa, H. Takamura, H. Ubukata, Y. Watanabe, K. Fujii, M. Yashima, A. Kuwabara, Y. Uchimoto and H. Kageyama, *Nat. Commun.*, 2021, **12**, 201.
79 X. Lu, G. Wu, J. W. Howard, A. Chen, Y. Zhao, L. L. Daemen and Q. Jia, *Chem. Commun.*, 2014, **50**, 11520.
80 Z. Deng, B. Radhakrishnan and S. P. Ong, *Chem. Mater.*, 2015, **27**, 3749.

This journal is © The Royal Society of Chemistry 2025